Journal of Crystal Growth 368 (2013) 1–5

Contents lists available at SciVerse ScienceDirect

Journal of Crystal Growth

journal homepage: www.elsevier.com/locate/jcrysgro

# Enhancement of epitaxial $LaNiO_3$ electrode on the ferroelectric property of La-doped $BiFeO_3/SrTiO_3$ artificial superlattice structure by rf sputtering

Shang-Jui Chiu [a,b], Yen-Ting Liu [c], Ge-Ping Yu [a,d,*], Hsin-Yi Lee [b,**], Jia-Hong Huang [a]

[a] Department of Engineering and System Science, National Tsing Hua University, Hsinchu 30013, Taiwan, ROC
[b] National Synchrotron Radiation Research Center, 101 Hsin-Ann Road, Hsinchu Science Park, Hsinchu 30076, Taiwan, ROC
[c] Program for Science and Technology of Accelerator Light Source, National Chiao Tung University, Hsinchu 300, Taiwan, ROC
[d] Institute of Nuclear Engineering and Science, National Tsing Hua University, Hsinchu 30013, Taiwan, ROC

ARTICLE INFO

*Article history:*
Received 11 June 2012
Accepted 17 December 2012
Communicated by: D.P. Norton
Available online 25 December 2012

*Keywords:*
A1. High resolution X-ray diffraction
A3. Physical vapor deposition process
B1. Oxide
B2. Ferroelectric materials

ABSTRACT

Improvement of ferroelectric property by $LaNiO_3$ (LNO) electrode on superlattice films was shown in this study. High quality asymmetric multiferroic 5 at% La-doped $BiFeO_3$ (BFO) and paraelectric $SrTiO_3$ (STO) superlattice structure was deposited on LNO electrode by rf magnetron sputtering system. High crystalline quality of the La-doped BFO/STO artificial superlattice structure on LNO electrode have been confirmed by clear main feature and satellite features around (0 0 2) STO substrate Bragg peak shown in (0 0 2) radial scan spectrum. The results of in-pane crystal truncation rod (CTR) spectrum and the rocking curve indicated that superlattice films with high crystal quality behaved in-plane strain closed to fully strained state on both LNO and Nb-doped STO electrode. The epitaxial relation between the La-doped BFO and STO layers in the superlattice was examined through a (1 0 3) azimuthal scan and (1 0 3) Lscan. The results show a four-fold symmetry and slight distorted of $\gamma$ angle of the BFO unit cell, confirming the pseudocubic structure of the La-doped $BiFeO_3$ structure. The measurement of hysteresis loops showed that La-doped BFO superlattice structure on LNO electrode behaved lower, but stable and saturated ferroelectric properties than that of films with Nb-doped STO substrate in our previous study. The measurement of resistivity and leakage current density of superlattice films demonstrated that resistivity of electrode is the main factor to determine the leakage properties of films. The superlattice films behaved larger piezoelectric coefficient ($d_{33}$) on LNO electrode than films on Nb-doped STO substrate, which indicated the enhancement of intrinsic ferroelectric properties in La-doped BFO/STO superlattice films.



## 1. Introduction

Multiferroic transition-metal oxides which are well known to behave ferroelectricity and magnetism have been extensively investigated because of their proprieties for prospective application like dynamic random-access memories and high-density nonvolatile random-access memories [1–3]. Bismuth iron oxide (BFO) is a lead-free multiferroic material with a large remnant polarization and antiferromagnetic properties and has been studied extensively in the past few decades. Previous study [4] has shown that epitaxial BFO thin films on single-crystal $SrTiO_3$ (STO) possess highly saturated ferroelectric hysteresis and great resistivity. Epitaxial BFO thin films show a greater Pr value than bulk BFO material, but serious problems with BFO including a large leakage current and ferroelectric unreliability because of a deviation from oxygen stoichiometry, which results in an increase of free charge carriers. Besides, defects such as Bi vacancies result from its substantial volatility [5,6]. An increased coercive field (*Ec*) and improved reliability are also critical challenges for $BiFeO_3$ as integrated microelectronic devices.

To solve the problem of BFO films, conducting perovskite bottom electrodes is a key factor to affect leakage properties, ferroelectric properties, and reliability of films. It has been reported that conductive perovskite electrodes with similar chemistry and structure to ferroelectric films like $SrRuO_3$ (SRO) [7–9], $YBa_2Cu_3O_{7-x}$ (YBCO) [10], $LaNiO_3$ (LNO) [11–13], and $BaPbO_3$ (BPO) [14], play an important role on ferroelectric enhancement of perovskite films. For those bottom electrode materials, it has been reported LNO that epitaxial growth on STO substrate by PLD method [15,16] and rf magnetron sputtering system [17] exhibits at relatively lower deposition temperatures

* Corresponding author at: Department of Engineering and System Science, National Tsing Hua University, Hsinchu 30013, Taiwan, ROC.
Tel.: +886 3 5715131x42376; fax: +886 3 5720724.
** Corresponding author. Tel.: +886 3 5780281; fax: +886 3 5789816.
*E-mail addresses:* gpyu@mx.nthu.edu.tw (G.-P. Yu), hylee@nsrrc.org.tw (H.-Y. Lee).

0022-0248/$ - see front matter Crown Copyright © 2012 Published by Elsevier B.V. All rights reserved.
http://dx.doi.org/10.1016/j.jcrysgro.2012.12.021

than other materials. Furthermore, the enhancement of (1 0 0)-oriented perovskite films by using LNO was also shown in previous study [11]; previous studies have shown that LNO could be used as bottom electrode to improve fatigue and aging properties of ferroelectric thin films [18,19].

The combination of effect in effective strain and ion doping on the structure and ferroelectric properties of perovskite materials has been studied in our previous research [20]. Base on those results, a further study of the integration of electrode effect and strain enhancement effect on BFO material with $La^{3+}$ doping is carried in this study. The objective of this work is to research the role of LNO electrode on the ferroelectric properties of La-doped BFO/STO superlattices films deposited by sputtering system.

## 2. Experimental details

Asymmetric ($t_{La-BFO}/t_{STO}$=4.0 nm/1.0 nm) 5% La-doped BFO/STO superlattice films with BFO and STO in sequence 10 layers were prepared by triple-gun rf-magnetron sputtering system on epitaxial growth (0 0 1) LNO electrode. Before deposition, the sputtering chamber was evacuated below $1.2\times10^{-4}$ Pa to avoid contamination. The LNO electrode was deposited on STO substrate with power density about 1.2 W cm$^{-2}$, and the total thickness of electrode is 100 nm. Sputtering was performed at power density about 1.5 W cm$^{-2}$ for both La-doped BFO and STO with a highly purified gas ($O_2$ 20%+Ar 80%) at a working pressure 2.05 Pa; the substrate temperature was fixed at 750 °C. With these parameters, the rates of growth of a deposited film for a La-doped BFO or STO sublayer were about 0.38 and 0.4 nm/min, respectively.

The high-resolution diffraction patterns were measured using a synchrotron as a source of X-ray at wiggler beamline BL-17B1 in the National Synchrotron Radiation Research Center (NSRRC), Hsinchu, Taiwan. The typical scattering vector resolution in the vertical scattering plane was set to $\sim1\times10^{-3}$ nm$^{-1}$ in these experiments.

For measurements of electrical properties, *Pt* top electrodes were sputtered onto the surface of the superlattice films near 25 °C. The ferroelectric hysteresis loop at frequency 1 kHz and 25 °C and leakage current measurements of La-doped BFO/STO superlattice films at various temperatures were measured with aixACCT TF-2000 analyzer. A commercial scanning probe micro microscope (CPII, Veeco) was used to perform measurement of piezoelectric coefficient ($d_{33}$). The resistivity of bottom electrode was given by Hall National Instruments NI-pxi-1042Q analyzer.

## 3. Results and discussion

To evaluate the effect of LNO electrode, the crystal structure of superlattice films with different electrode has to be conformed firstly. Fig. 1 plots the (0 0 *L*) radial scan of La-doped $BFO_{4\ nm}$/$STO_{1\ nm}$ superlattice films with LNO electrode deposited on STO substrate and Nb-doped STO electrode, respectively. The diffraction patterns of films with a clear main line and satellite lines with order periodicity, which consisting with fitting results of X-ray reflection pattern in our previous study [20], indicate that the superior crystalline quality and interface quality of superlattice structure with LNO electrode. With total thickness of 40 nm, the superlattice films deposited on Nb-doped STO electrode behave clearly discernible Pendellösung fringes. The fringes are not distinguishable in the superlattice film with a much thicker LNO electrode of 140 nm.

Fig. 2(a) displays the crystal truncation-rod spectra of the superlattice films in [*H* 0 0] direction. Similar with the result of

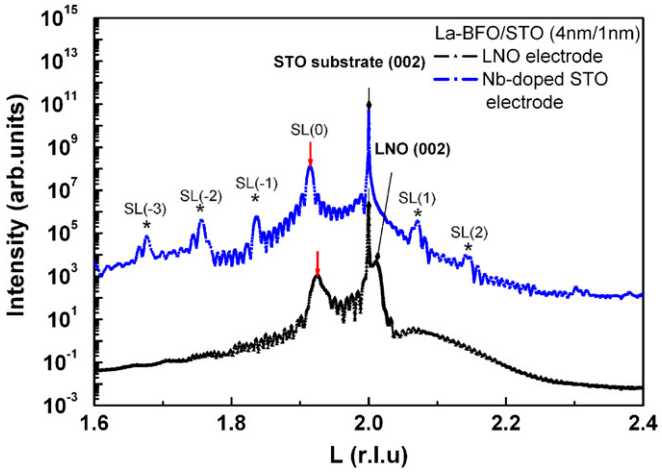


**Fig. 1.** (0 0 2) radial scan of La-doped BFO/STO superlattice films for (0 0 *L*) spectrum.

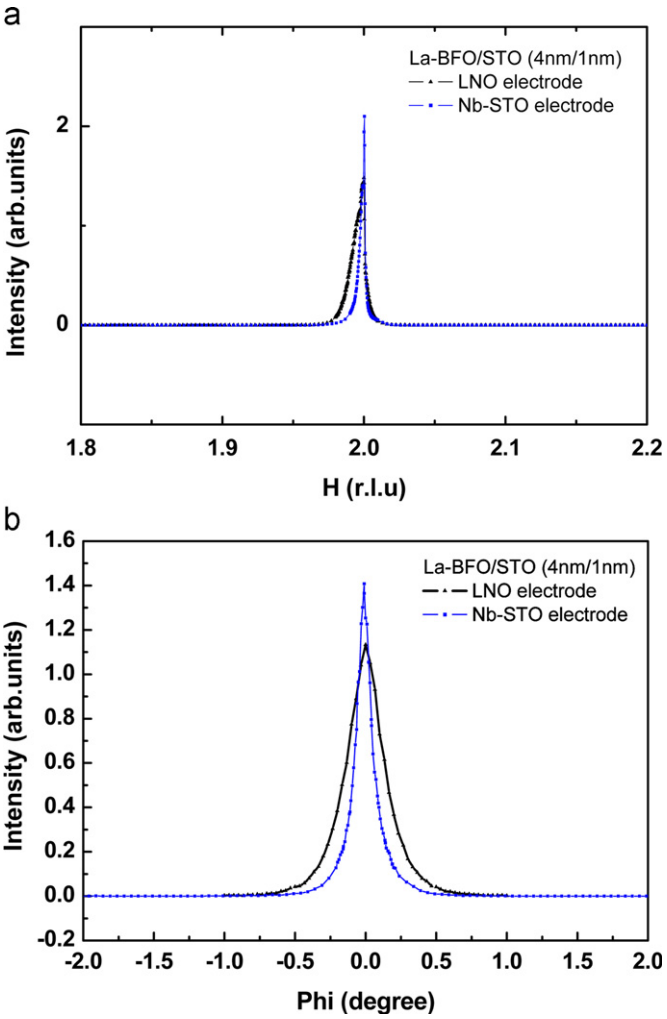


**Fig. 2.** (a) In-plane (*H* 0 0) crystal truncation-rod spectra of La-doped BFO/STO superlattice films (b) Full width at half-maximum (FWHM) of the in-plane rocking curves of La-doped BFO/STO superlattice films.

superlattice films deposited on Nb-doped STO substrate, the superlattice films deposited on LNO electrode yield a diffraction peak which overlaps with peaks of the STO substrate, revealing that the La-doped BFO/STO superlattice is well-strained by

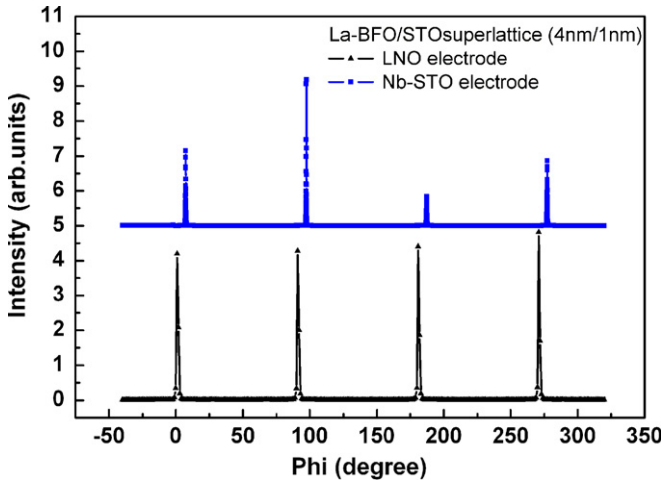


**Fig. 3.** (1 0 3) Azimuthal scan ($\Phi$ scan) pattern of La-doped BFO/STO superlattice.

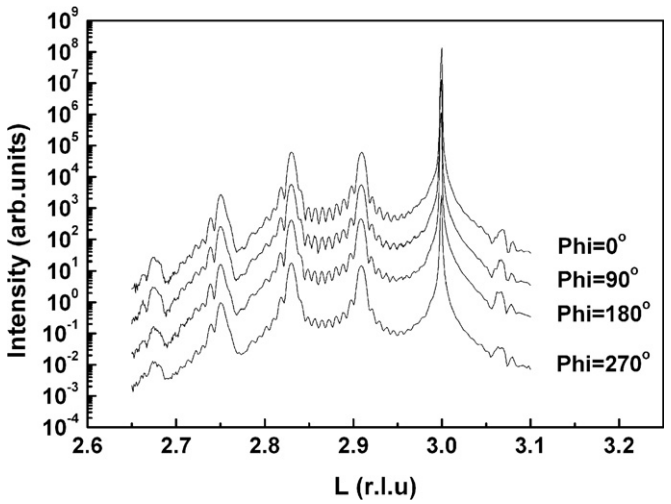


**Fig. 4.** Radial scan of (1 0 3) diffraction peak of La-doped BFO/STO superlattice films on Nb-doped STO substrate spectrum along (0 0 $L$) direction.

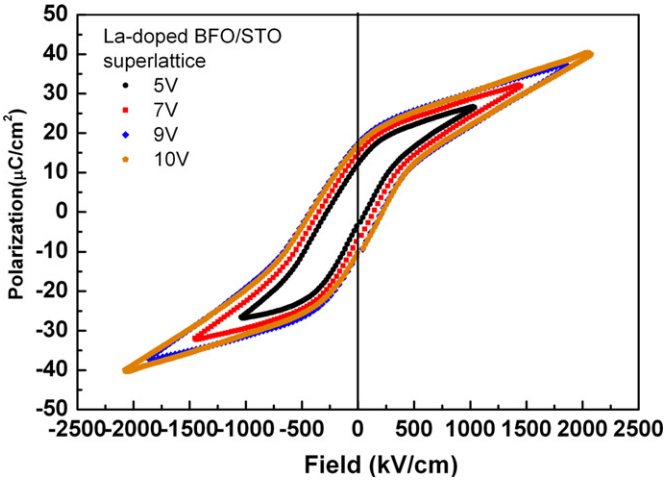


**Fig. 5.** Electric hysteresis loops of La-doped BFO/STO superlattice films deposited on LNO and Nb-doped STO electrode.

the LNO electrode; only slight relaxation of strain is observed. The horizontal lattice parameter of a superlattice in a cubic system is calculated by the equation $a=(H\sin\theta)\lambda/2$. The superlattice films with LNO electrode have a horizontal lattice parameter smaller than the lattice constant of bulk BFO (0.396 nm), which shows the compression of the BFO lattice by the LNO electrode. Given by the equation $\varepsilon_{xx}=(a_x-a_{x0})/a_{x0}$, the superlattice films with LNO electrode and Nb-doped STO electrode behave a similar in-plane strain $\sim$1.3%, which approaches the critical value of 1.42% associated with a fully strained BFO sublayer. The full width at half-maximum (FWHM) of the in-plane rocking curves of La-doped BFO/STO superlattice films is given in Fig. 2(b). Superlattice films deposited on LNO electrode behave slightly broadening of rocking curves comparing with that of films deposited on Nb-doped STO electrode, which reveals lower but similar quality of superlattice films on LNO electrodes.

The azimuthal scan ($\Phi$ scan) performed in the vicinity of the STO (1 0 3) Bragg peak is given in Fig. 3. The azimuthal diffraction patterns of superlattice films deposited on Nb-STO electrode and LNO electrode clearly exhibit a four-fold symmetry with the same orientation. These results constitute firm evidence for strong epitaxy of the deposited layer on the substrate; no other peaks are observed in the intervals between the four peaks, indicating a perfect alignment of $\vec{a}$ and $\vec{b}$ axes of BFO and STO unit cells along those of the STO substrate.

Previous studies [21] have demonstrated that the epitaxial growth Perovskite-type films behave depth-dependent phase transformation. It was also shown that epitaxial growth Perovskite-type materials could exhibit various $\gamma$ angles [22]. Although the azimuthal scan demonstrates that the superlattice films deposited on LNO electrode exhibit excellent pseudo-cubic crystal structure that all diffraction peaks have similar intensity, the observable difference of intensity in each of diffraction peak could be found in azimuthal diffraction patterns of a superlattice film deposited on Nb-doped STO films. To further confirm the structure of superlattice films, the critical study to determinate $\gamma$ angle of BFO crystal was made. Fig. 4 presents the radial scan of (1 0 3) peak along surface normal ($L$) direction of superlattice films with various Phi angle (0°, 90°, 180°, 270°). Without relative shift of main peak in this pattern, the overlapping of diffraction pattern with four phi degrees (with very small difference of $L$-index coordination) demonstrates the pseudo-cubic crystal structure without shift of $\gamma$ angle in the superlattice films. The difference of intensity for each peak in azimuthal scan may resulted from excellent crystal quality of superlattice films; with high crystal quality similar with single crystal, superlattice films would exhibit intense variation of intensity of diffraction even with such a unconsidered difference in $\gamma$ angle.

Electric hysteresis loops of a La-doped BFO/STO superlattice film with LNO electrode are shown in Fig. 5. Even with the lower polarization value of films comparing with that of films deposited on Nb-doped STO electrode shown in our previous study [20], the typical shape of the hysteresis loops with polarization value ranging from 16 $\mu C/cm^{-2}$ to 28.83 $\mu C/cm^{-2}$ showed a stable polarization value with increasing applying electrical voltage, which prove that the superlattice films is saturated with applied voltage larger than 7 V.

Fig. 6 plots the current density as a function of electric field for La-doped BFO/STO superlattice films. To investigate the electrical properties of electrode on superlattice films, the current density of superlattice films deposited on $SrRuO_3$ electrode (the same thickness with LNO electrode) was also shown. Superlattice films deposited on Nb-doped STO electrode behaves two-order lower leakage density than films with LNO electrode, and the superlattice films with LNO electrode also behave about two-order lower leakage current density than superlattice films with SRO electrode. It seems that the superlattice films with Nb-doped STO electrode exhibits the highest leakage quality, but the Hall measurement of resistivity indicates that the variation of leakage

current is not resulted from superlattice film. The Hall analysis shows the resistivity of Nb-doped electrode is $3.83 \times 10^4\ \Omega$-cm, and the resistivity of LNO electrode and SRO electrode is $2.76 \times 10^2\ \Omega$-cm and 25.1 Ω-cm. The negative-related relationship between leakage current and resistivity is observed; with two-order larger resistivity of bottom electrode, superlattice films exhibit about two-order lower leakage current. These results demonstrate that the difference resistivity of the electrode is the main factor to cause the variation of leakage current density.

It is known that the ferroelectric materials always behave piezoelectric properties [23], and the relationship of superlattice films between polarization value and piezoelectric coefficient has been proved in our early study. The ferroelectric behavior of the La-doped BFO/STO superlattice films on each electrode could also be estimated by the piezoelectric properties of superlattice films. The piezoelectric coefficient ($d_{33}$) of the standard BFO films and superlattice films is given in Fig. 7. Superlattice films with LNO electrode shows higher piezoelectric coefficient (46 pm/V) than those of films on Nb-doped STO electrode (28.1 pm/V). This result constitutes evidence of enhancement ferroelectric properties of superlattice films by using LNO electrode.

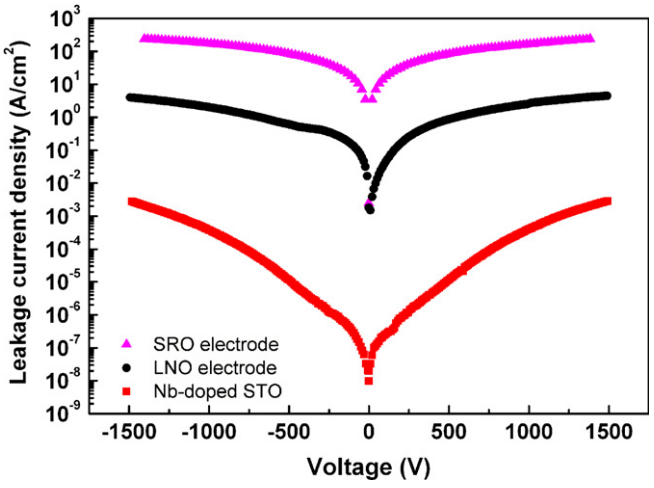


**Fig. 6.** Leakage current density of La-doped BFO/STO superlattice films with LNO, SRO, and Nb-doped STO electrode.

It has been shown in our previous study [20] that La-doped BFO/STO superlattice films deposited on Nb-doped STO bottom electrode display great crystalline quality, small leakage current density and good ferroelectric properties with great polarization value. However, lower piezoelectric coefficient ($d_{33}$) of superlattice films with Nb-doped STO electrode is also observed in this study. On the other hand, even with lower polarization value, superlattice films deposited on LNO electrode behave saturated and stable hysteresis loops and large piezoelectric coefficient ($d_{33}$). It is known that the "polarization" determined by electric hysteresis loops, so called the electric displacement (D), could be given by following equation [24]:

$$D = \varepsilon_0 \varepsilon_r E + P_s \quad (1)$$

where $\varepsilon_r$ the dielectric constant of the ferroelectric film, $E$ is is the applied electric field, and. $P_S$ is the spontaneous polarization. The electric hysteresis loops of superlattice films contain the total amount of electric displacement of superlattice films including ferroelectricity and dielectricity [25]. When superlattice films were deposited on Nb-doped STO electrode, Nb-STO electrode with large resistivity may lead to huge amount of polarization value resulted from dielectricity of electrode. So, even with lower $d_{33}$ coefficient, superlattice films deposited on Nb-doped STO electrode behave much higher but non-saturated polarization value and lower leakage current density comparing with that of films on LNO electrode. These results demonstrate that the

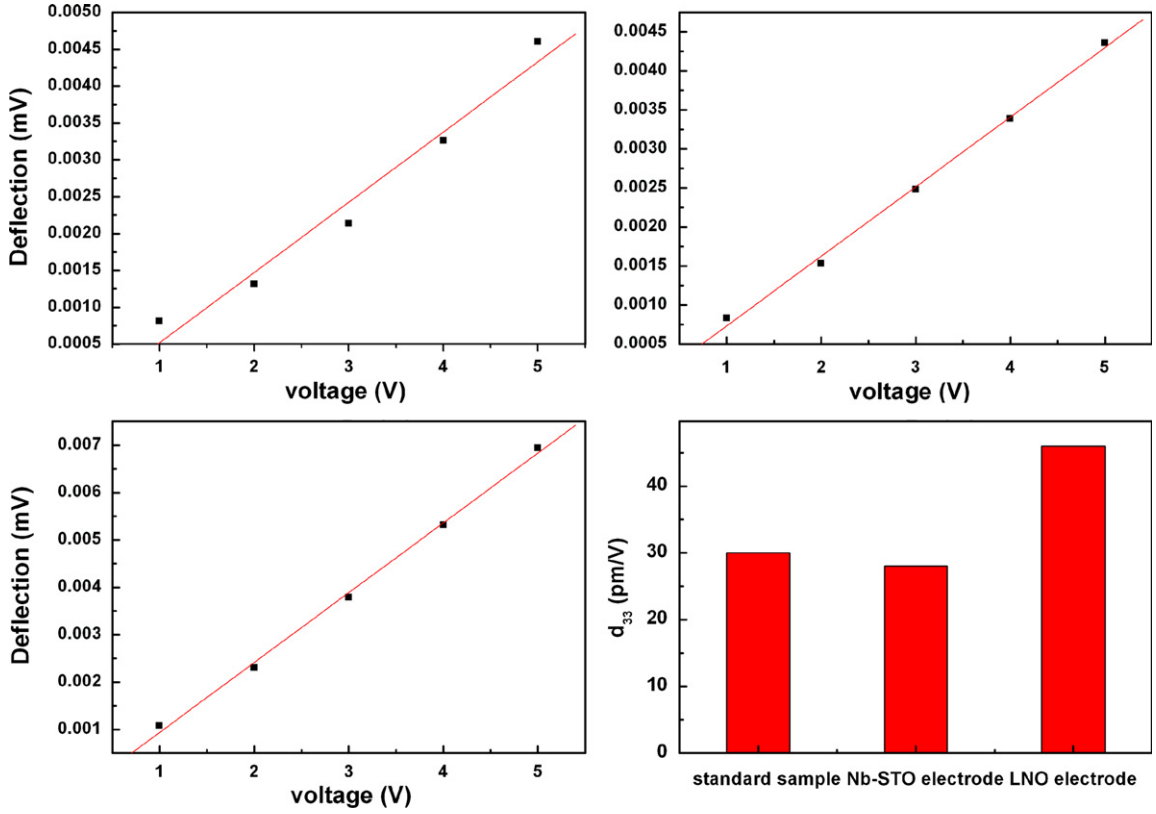


**Fig. 7.** Piezoelectric coefficient $d_{33}$ values of standard BFO sample and superlattice films.

conducting perovskite bottom electrodes, which is an important factor as strain state and crystalline quality of films, is correlated with remnant polarization and $d_{33}$ coefficient films.

## 4. Conclusions

High quality La–doped BFO/STO superlattice structure was deposited on $LaNiO_3$ electrode to verify the effect of bottom electrode on the ferroelectric properties. The superlattice structure of the films on LNO electrode has been proofed by clear main feature and satellite features shown in (0 0 2) radial scan spectrum. In-pane crystal truncation rod (CTR) spectrum and the rocking curve revealed that superlattice films with high crystal quality behaved and in-plane strain closed to superlattice films deposited on LNO electrode and Nb-doped STO electrode. The epitaxial relation of the superlattice was estimated through a (1 0 3) azimuthal scan and (1 0 3) radial scan along L direction, which indicate a four-fold symmetry of the pseudocubic structure BFO cell. The hysteresis loops present that La-doped BFO superlattice structure on LNO electrode behaved lower, but much stable and saturated ferroelectric property than that of films with Nb-STO substrate. The results of piezoelectric coefficient measurement demonstrated that the superlattice films behaved better ferroelectric properties on LNO electrode than films Nb-STO substrate. Even with lower polarization values and larger leakage current, La-doped BFO/STO superlattice films with LNO electrode behave much better and intrinsic ferroelectric properties.

## Acknowledgement

National Science Council of Republic of China supported this work under contract NSC 99–2221-E-213-002-MY2. The ferroelectric properties were measured in the Ferroelectric Laboratory, Fu Jen Catholic University

The measurement of piezoelectric coefficient ($d_{33}$) is supported by Applied Nano Science Laboratory, Department of Physics, National Cheng Kung University.

## References

[1] G.A. Smolenskii, I. Chupis, Soviet Physics Uspekhi 25 (1982) 475.
[2] J. Zhang, D. Cui, H. Lu, Z. Chen, Y. Zhou, L. Li, G. Yang, S. Martin, P. Hess, Japanese Journal of Applied Physics 76 (1997) 362.
[3] C.S. Hsi, F.Y. Hsiao, N.C. Wu, M.C. Wang, Japanese Journal of Applied Physics 42 (2003) 544.
[4] J. Wang, J. Neaton, H. Zheng, V. Nagarajan, S. Ogale, B. Liu, D. Viehland, V. Vaithyanathan, D. Schlom, U. Waghamare, N. Spaldin, K. Rabe, M. Wuttig, R. Ramesh, Science 299 (2003) 1719.
[5] H. Bea, M. Bibes, A. Barthelemy, K. Bouzehouane, E. Jacquet, A. Khodan, J.P. Contour, S. Fusil, F. Wyczisk, A. Forget, D. Lebeugle, D. Colson, M. Viret, Applied Physics Letters 87 (2005) 072508.
[6] T. Shimuta, O. Nakagawara, T. Makino, S. Arui, H. Tabata, T. Kawai, Journal of Applied Physics 91 (2002) 2290.
[7] J. Wang, H. Zheng, Z. Ma, S. Prasertchoung, M. Wuttig, R. Droopad, J. Yu, K. Eisenbeiser, R. Ramesh, Applied Physics Letters 85 (2004) 2574.
[8] H.N. Al-Shareef, A.I. Kingon, X. Chen, K.R. Buller, O. Auciello, Journal of Materials Research 9 (1994) 2968.
[9] D.P. Vijat, S.B. Desu, Journal of the Electrochemical Society 140 (1993) 2640.
[10] R. Ramesh, W.K. Chan, B. Wilkens, H. Gilchrist, T. Sands, J.M. Tarascon, V.G. Keramidas, Applied Physics Letters 61 (1992) 1537.
[11] M.S. Chen, T.B. Wu, J.M. Wu, Applied Physics Letters 68 (1996) 1430.
[12] J.H. Kim, H. Funakubo, H. Ishiwara, Japanese Journal of Applied Physics 50 (2011) 051501.
[13] J. Wu, J. Wang, Journal of Applied Physics 107 (2010) 034103.
[14] Y.R. Luo, J.M. Wu, Applied Physics Letters 79 (2001) 3669.
[15] W.B. Wu, K.H. Wong, P.W. Chan, Physica C 297 (1998) 247.
[16] N. Wakiya, T. Azuma, K. Shinozaki, N. Mizutani, Thin Solid Films 410 (2002) 114.
[17] C.C. Yang, M.S. Chen, T.J. Hong, C.M. Wu, T.B. Wu, Applied Physics Letters 66 (1995) 2643.
[18] R. Ramesh, H. Gilchrist, T. Sands, J.M. Tarascon, V.G. Keramidas, Applied Physics Letters 63 (1993) 3592.
[19] Q. Gan, R.A. Rao, C.B. Eom, Applied Physics Letters 72 (1998) 978.
[20] S.J. Chiu, Y.T. Liu, G.P. Yu, H.Y. Lee, J.H. Huang, Thin Solid Films (2012), http://dx.doi.org/10.1016/j.tsf.2012.02.033.
[21] H.J. Liu, C.W. Liang, W.I. Liang, H.J. Chen, J.C. Yang, C.Y. Peng, G.F. Wang, F.N. Chu, Y.C. Chen, H.Y. Lee, L. Chang, S.J. Lin, Y.H. Chu, Physical Review B 85 (2012) 014104.
[22] D. Kan, Y. Shimakawa, Crystal Growth and Design 11 (2011) 5483.
[23] A.J. Moulson and J.M. Herbert, Electroceramics Materials, Properties, Applications.
[24] I. Boerasu, L. Pintilie, M. Pereira, M.I. Vasilevskiy, M.J.M. Gomes, Journal of Applied Physics 93 (2003) 4776.
[25] J.F. Scott, Journal of Physics: Condensed Matter 20 (2008) 021001.